Near-Field Line-of-Sight Communication with Massive Movable Antennas

Shicong Liu and Xianghao Yu
Department of Electrical Engineering, City University of Hong Kong, Hong Kong
Email: sc.liu@my.cityu.edu.hk, alex.yu@cityu.edu.hk

***Abstract*—The proliferation of the sixth generation (6G) networks demands innovative antenna technologies to fully unlock spatial degrees of freedom. Large-scale position-reconfigurable antenna (PRA) arrays have emerged as a promising solution, while existing antenna position design approaches often suffer from high computational complexity and neglect the near-field effect. In this paper, we propose efficient methods to determine the antenna positions for near-field line-of-sight communication. Specifically, by transforming the antenna positions into the angular domain, we reformulate the achievable rate maximization problem as a Vandermonde matrix determinant maximization problem, which is known as a *weighted Fekete problem*, whose optimal solution can be obtained by off-the-shelf solvers. To further reduce the computational complexity, we propose a greedy algorithm to find the asymptotically optimal antenna positions accommodating practical physical constraints. Simulation results demonstrate that the proposed scheme yields a considerable achievable rate gain compared to the conventional uniform linear array scheme in the near-field region with up to $35\times$ reduction in design complexity.**

I. Introduction

Beyond fifth generation (B5G) and sixth generation (6G) networks demand unprecedented data rates, reliability, and massive connectivity [1]. Accommodating these stringent requirements calls for innovative strategies to unlock and exploit the spatial degrees of freedom (DoFs), which are pivotal in advancing the performance of wireless communication systems. In recent years, massive multiple-input multiple-output (MIMO) antenna systems have proven highly effective in enhancing spatial multiplexing efficiency. To further extend their capabilities, large-scale reconfigurable antenna technology, such as reconfigurable intelligent surfaces (RIS) [2], presents energy-efficient solutions for boosting spatial multiplexing capabilities [3].

Driven by recent breakthroughs in mechanical innovations and antenna technologies, position-reconfigurable antenna (PRA) technologies such as movable antennas (MA) [4], fluid antenna systems (FAS) [5], and pinching antennas [6], have garnered increasing interests from both academia and industry. These antenna architectures enable more favorable propagation environments and offer more precise manipulation of radiation patterns, thereby improving overall communication performance. With the widespread adoption of massive MIMO arrays, there is an urgent need for optimal design strategies specifically tailored to PRA arrays with a large number of elements.

Previous works have validated the remarkable performance gains of PRAs compared to conventional fixed-position antennas in wireless systems [7]–[11]. However, significant gaps remain in current optimization-oriented research. First of all, existing works heavily rely on numerical optimization algorithms [8]–[11], which may entail excessively high computational complexity due to the intrinsic iterative procedures and nested loops of such algorithms. Besides, in massive MIMO systems, the aperture of antenna arrays becomes so large that near-field effects can no longer be ignored [12]. Although it offers additional spatial DoFs to be leveraged, the spherical wave model introduces substantial challenges in system design, and thus, only limited attention has been paid to this regime in existing studies [7]–[9], [11].

In this paper, we address the efficient antenna placement problem in the near-field line-of-sight (LoS) scenario, and also tackle the computational complexity issue associated with the conventional numerical methods. In particular, we first transform the position of antennas into the angular domain, and formulate the corresponding position optimization problem into a *weighted Fekete problem*, which is proved to be a concave problem and can be solved by mathematical tools such as CVX. We further develop a greedy algorithm based on the Leja sequence by incrementally constructing the antenna set via a series of low-dimensional sub-problems, which not only asymptotically approaches the optimal antenna positions but also significantly reduces the computational complexity. Numerical results clearly demonstrate the performance improvement of the proposed greedy method over various benchmark schemes. Moreover, as the number of antennas increases, the proposed greedy algorithm asymptotically approaches the solution provided by CVX, while reducing computational complexity by up to three orders of magnitude.

Notations: We use normal-face letters to denote scalars and lowercase (uppercase) boldface letters to denote column vectors (matrices). The element at the k-th row and the m-th column of matrix $\mathbf{H}$ is denoted as $\mathbf{H}[k,m]$, and the n-th element in the vector $\mathbf{h}$ is denoted by $\mathbf{h}[n]$. $\mathrm{diag}(\mathbf{h})$ generates a square matrix with the entries of $\mathbf{h}$ on its main diagonal. The superscripts $(\cdot)^T$, $(\cdot)^*$, and $(\cdot)^H$ represent the transpose, conjugate, and conjugate transpose operators, respectively. $\det(\cdot)$, and $\mathrm{Tr}(\cdot)$ denote the determinant and trace operators, respectively. The imaginary unit is represented as $\jmath$ such that

This work was supported in part by the NSFC Young Scientists Fund No. 62301468, and in part by the Hong Kong Research Grants Council under Grant No. 21215423.

Simulation codes for reproducing this work are available at: https://github.com/scliubit/Near-Field-Movable-Antenna-ICC

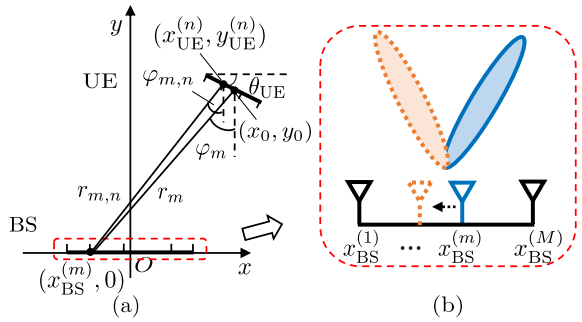

Fig. 1. (a) The considered near-field communication scenario and (b) the schematic diagram of massive MAs, with the 1-st and M-th antennas fixed at the edges.

$\jmath^2 = -1$. $\mathbb{R}$ denotes the set of real numbers.

II. System Model

In this section, we describe the system model adopted for the antenna position design, including both the massive MA configuration and the corresponding channel model.

A. Massive Position-Reconfigurable Antennas

Consider a point-to-point massive MIMO downlink transmission scenario with M MAs[1] at the base station (BS) side and N fixed-position antennas at the user equipment (UE) side. As shown in Fig. 1, the Cartesian coordinate system is established with the centroid of the BS array coinciding with its origin $O(0,0)$, while the BS array aligns along the x-axis. The coordinates of the m-th element on the BS array and the n-th element on the UE array are given by $(x_{\rm BS}^{(m)}, 0)$ and $(x_{\rm UE}^{(n)}, y_{\rm UE}^{(n)})$, respectively.

In this paper, the x coordinates of BS antenna elements, i.e., $\{x_{\rm BS}^{(1)}, x_{\rm BS}^{(2)}, \cdots, x_{\rm BS}^{(M)}\}$, are strictly increasing specified by

$$-\frac{A}{2} = x_{\rm BS}^{(1)} < x_{\rm BS}^{(2)} < \cdots < x_{\rm BS}^{(M)} = \frac{A}{2}, \tag{1}$$

where A denotes the standard BS array aperture.

B. Channel Model

We adopt the spherical wave model [12] to characterize the near-field wireless channel in this paper. Specifically, the spatial response between the m-th antenna on the BS array and the n-th antenna on the UE array is modeled by

$$h\left(r_{m,n}\right) = \frac{e^{\jmath\kappa r_{m,n}}}{r_{m,n}}, \tag{2}$$

where $r_{m,n}$ denotes the distance between the m-th and n-th antenna elements on the BS and UE arrays, respectively, given by

$$r_{m,n} = \sqrt{\left(y_{\rm UE}^{(n)}\right)^2 + \left(x_{\rm UE}^{(n)} - x_{\rm BS}^{(m)}\right)^2}, \tag{3}$$

and $\kappa = 2\pi/\lambda$ is the wavenumber with λ being the carrier wavelength.

[1]To simplify the problem and promote practicality, this work only focuses on MAs at BS, with fixed antenna elements at the UE side. However, due to the spatial reciprocity of the channel model, the proposed methodology can also be extended to UEs with MAs.

As the LoS component is generally not likely to experience blockage and delivers a much stronger signal than the non-line-of-sight (NLoS) counterparts in the near-field region [13], the near-field channel is mainly dominated by the LoS component, which can be expressed as

$$\mathbf{H}_{\mathbf{x}}[n,m] = h\left(r_{m,n}\right). \tag{4}$$

In (4), $\mathbf{x} = [x_{\rm BS}^{(1)}, x_{\rm BS}^{(2)}, \cdots, x_{\rm BS}^{(M)}]$ denotes the position vector of the BS antenna elements on the x-axis. Hence, the downlink channel matrix is a function of $\mathbf{x}$.

III. Problem Formulation and Analysis

In this section, we reformulate the near-field achievable rate maximization problem as a *weighted Fekete problem*, where the coordinates of the antenna elements are transformed into the angular domain and treated as optimization variables.

With a given antenna position vector $\mathbf{x}$, the achievable rate is given by

$$R_{\mathbf{x}} = \log_2 \det\left(\mathbf{I}_N + \frac{1}{\sigma_{\rm n}^2}\mathbf{H}_{\mathbf{x}}\mathbf{Q}\mathbf{H}_{\mathbf{x}}^H\right), \tag{5}$$

where σ_n^2 is the power of additive white Gaussian noise (AWGN), and $\mathbf{Q}$ is the transmit covariance matrix. In this paper, since our primary focus is on the performance gains introduced by the MA, we assume an isotropic transmission with $\mathbf{Q} = \frac{P_{\rm T}}{M}\mathbf{I}_M$, where $P_{\rm T}$ denotes the total transmit power. Therefore, the achievable rate is further given by

$$R_{\mathbf{x}} = \log_2 \det\left(\mathbf{I}_N + \frac{\rho}{M}\mathbf{H}_{\mathbf{x}}\mathbf{H}_{\mathbf{x}}^H\right), \tag{6}$$

where $\rho = \frac{P_{\rm T}}{\sigma_{\rm n}^2}$ denotes the signal-to-noise ratio (SNR). Our objective is to determine the optimal antenna positions $\mathbf{x}$ such that, by reorganizing the intrinsic structure of the channel matrix $\mathbf{H}_{\mathbf{x}}$, more orthogonal transmission modes can be excited and fully exploited to achieve a higher achievable rate. Accordingly, the overall design problem can be formulated as

$$\begin{aligned} \mathcal{P}_1: \quad & \max_{\mathbf{x}} \quad R_{\mathbf{x}} \\ & \text{s.t.} \quad \mathbf{x}[M] = -\mathbf{x}[1] = \frac{A}{2}, \\ & \qquad \mathbf{x}[m+1] - \mathbf{x}[m] > 0, \quad 1 \le m \le M-1, \end{aligned} \tag{7}$$

where the first constraint confines the moving area within the aperture $[-A/2, A/2]$, while the second enforces the ordered structure of $\mathbf{x}$ in (1).

In the near-field region, the received signal exhibits a much slighter fading effect compared to far-field region, and hence, the high SNR $\rho \gg 1$ holds. The original achievable rate objective in (5) can then be accurately approximated by

$$R_{\mathbf{x}} \simeq \log_2 \det\left(\rho\mathbf{H}_{\mathbf{x}}\mathbf{H}_{\mathbf{x}}^H\right) \triangleq \tilde{R}_{\mathbf{x}}. \tag{8}$$

Revisiting the channel model in (4), we need to derive the distance terms $r_{m,n}$ to accomplish the formulation. As shown in Fig. 1, the centroid coordinate of the UE array is (x_0, y_0), and the coordinate of the n-th antenna on the UE array is then given by

$$\begin{cases} x_{\rm UE}^{(n)} & = x_0 + d_n \cos\theta_{\rm UE} \\ y_{\rm UE}^{(n)} & = y_0 + d_n \sin\theta_{\rm UE} \end{cases}, \tag{9}$$

where θ_{UE} is the azimuth angle of the UE array, and d_n denotes the relative distance from the n-th element to the centroid (x_0, y_0). By substituting (9) into (3), we have

$$\begin{aligned} & r_{m,n} \\ &= \sqrt{\left(y_0+d_n\sin\theta_{\mathrm{UE}}\right)^2+\left(x_0+d_n\cos\theta_{\mathrm{UE}}-x_{\mathrm{BS}}^{(m)}\right)^2} \\ &= \sqrt{r_m^2+2d_n\left(y_0\sin\theta_{\mathrm{UE}}+\left(x_0-x_{\mathrm{BS}}^{(m)}\right)\cos\theta_{\mathrm{UE}}\right)+d_n^2} \end{aligned} \tag{10}$$

where $r_m^2 = y_0^2+(x_0-x_{\mathrm{BS}}^{(m)})^2$ represents the squared distance from the centroid of the UE to the m-th element on the BS array. According to Fig. 1, in a typical near-field communication scenario, the communication distance r_m is far larger than the aperture of the UE array, i.e., $r_m \gg \max(d_n)$. Therefore, the second-order small quantity d_n^2 in (10) is negligible and we perform a binomial expansion [12] as

$$\begin{aligned} r_{m,n} &\simeq r_m+\frac{d_n}{r_m}\left(y_0\sin\theta_{\mathrm{UE}}+\left(x_0-x_{\mathrm{BS}}^{(m)}\right)\cos\theta_{\mathrm{UE}}\right) \\ &\triangleq \tilde{r}_{m,n}. \end{aligned} \tag{11}$$

Since we have $\cos\varphi_m = y_0/r_m$ and $\sin\varphi_m = (x_{\mathrm{BS}}^{(m)} - x_0)/r_m$, (11) further yields

$$\begin{aligned} \tilde{r}_{m,n} &= r_m + d_n\left(\sin\theta_{\mathrm{UE}}\cos\varphi_m-\cos\theta_{\mathrm{UE}}\sin\varphi_m\right) \\ &= y_0\sec\varphi_m + d_n\sin\left(\theta_{\mathrm{UE}}-\varphi_m\right). \end{aligned} \tag{12}$$

Note that in the spherical wave model (2), the distance term in the phase has a significantly greater impact on the channel characteristics than the distance term in the denominator. This is because the wavenumber $\kappa = 2\pi/\lambda$ is typically very large, especially at high carrier frequencies. In contrast, the physical size of the UE array is generally small, resulting in only limited absolute variation in distance $\tilde{r}_{m,n}$ across different UE antennas. To facilitate tractable analysis, we therefore neglect the d_n-dependent variation in $\tilde{r}_{m,n}$, and retain only r_m in the denominator of (2). Substituting the distance terms $\tilde{r}_{m,n}$ and r_m into the phase and denominator of the channel model (2), respectively, we have

$$\mathbf{H}_{\mathbf{x}}[n,m] \simeq \frac{e^{\jmath\kappa(r_m+d_n\sin(\theta_{\mathrm{UE}}-\varphi_m))}}{r_m} \triangleq \tilde{\mathbf{H}}_{\mathbf{x}}[n,m]. \tag{13}$$

Since the denominator r_m depends only on the antenna index m of the BS array, the approximated channel matrix $\tilde{\mathbf{H}}_{\mathbf{x}}$ can be decomposed by

$$\tilde{\mathbf{H}}_{\mathbf{x}} = \mathbf{P}\mathbf{D}_{\mathrm{T}}, \tag{14}$$

where $\mathbf{D}_{\mathrm{T}}$ is an M-dimensional diagonal matrix given by

$$\mathbf{D}_{\mathrm{T}} = \mathrm{diag}\left(\left[\frac{e^{\jmath\kappa r_1}}{r_1}, \frac{e^{\jmath\kappa r_2}}{r_2}, \cdots, \frac{e^{\jmath\kappa r_M}}{r_M}\right]\right), \tag{15}$$

and $\mathbf{P}$ contains only the phase terms with cross-dependence between m and n, to which we employ Taylor expansion [14] for its (n,m)-th entry as

$$\begin{aligned} \mathbf{P}[n,m] &= e^{-\jmath\kappa d_n\sin(\varphi_m-\theta_{\mathrm{UE}})} \\ &= \sum_{k=0}^{\infty}\frac{\left(-\jmath\kappa d_n\sin\left(\varphi_m-\theta_{\mathrm{UE}}\right)\right)^k}{k!}. \end{aligned} \tag{16}$$

Hence, matrix $\mathbf{P}$ can be decomposed as

$$\mathbf{P} = \mathbf{V}_{\mathrm{R}}\mathbf{\Sigma}\mathbf{V}_{\mathrm{T}}^H, \tag{17}$$

with $\mathbf{\Sigma} = \mathrm{diag}\left((-\jmath\kappa)^0/0!, (-\jmath\kappa)^1/1!, \cdots\right)$ as a diagonal matrix with *infinite* columns, while $\mathbf{V}_{\mathrm{T}}$ and $\mathbf{V}_{\mathrm{R}}$ are Vandermonde matrices with *infinite* columns at the BS and UE sides, respectively, sharing a similar form as

$$\mathbf{V}_{\mathrm{T}} = \begin{bmatrix} 1 & \sin\left(\varphi_1-\theta_{\mathrm{UE}}\right) & \sin^2\left(\varphi_1-\theta_{\mathrm{UE}}\right) & \cdots \\ 1 & \sin\left(\varphi_2-\theta_{\mathrm{UE}}\right) & \sin^2\left(\varphi_2-\theta_{\mathrm{UE}}\right) & \cdots \\ \vdots & \vdots & \vdots & \cdots \\ 1 & \sin\left(\varphi_M-\theta_{\mathrm{UE}}\right) & \sin^2\left(\varphi_M-\theta_{\mathrm{UE}}\right) & \cdots \end{bmatrix} \tag{18}$$

and

$$\mathbf{V}_{\mathrm{R}} = \begin{bmatrix} 1 & d_1 & d_1^2 & \cdots \\ 1 & d_2 & d_2^2 & \cdots \\ \vdots & \vdots & \vdots & \cdots \\ 1 & d_N & d_N^2 & \cdots \end{bmatrix}. \tag{19}$$

Note that the absolute values of the diagonal entries of $\mathbf{\Sigma}$

$$\left|\frac{(-\jmath\kappa)^k}{k!}\right| \propto \sqrt{k+1}\left(\frac{\kappa e}{k+1}\right)^{k+1} \tag{20}$$

decay factorially with the value of k. Therefore, we can truncate the matrices $\mathbf{\Sigma}$, $\mathbf{V}_{\mathrm{T}}$, and $\mathbf{V}_{\mathrm{R}}$ to M columns, with negligible error (when M is large) as

$$\mathbf{P} \simeq \underline{\mathbf{V}}_{\mathrm{R}}^{(M)}\underline{\mathbf{\Sigma}}^{(M)}\left(\underline{\mathbf{V}}_{\mathrm{T}}^{(M)}\right)^H \triangleq \underline{\mathbf{P}}^{(M)}. \tag{21}$$

Substituting (13), (14), and (21) into (8), we further simplify the objective function $\tilde{R}_{\mathbf{x}}$ in the near-field region as

$$\begin{aligned} & \tilde{R}_{\mathbf{x}} = \log_2\det\left(\rho\mathbf{H}_{\mathbf{x}}\mathbf{H}_{\mathbf{x}}^H\right) \\ &\simeq N\log_2\rho + \log_2\det\left(\mathbf{D}_{\mathrm{T}}\mathbf{D}_{\mathrm{T}}^H\right) + \log_2\det\left(\underline{\mathbf{P}}^{(M)}\left(\underline{\mathbf{P}}^{(M)}\right)^H\right) \\ &= R_0 + \log_2\det\left(\mathbf{D}_{\mathrm{T}}\mathbf{D}_{\mathrm{T}}^H\right) + \log_2\det\left(\left(\underline{\mathbf{V}}_{\mathrm{T}}^{(M)}\right)^H\underline{\mathbf{V}}_{\mathrm{T}}^{(M)}\right), \end{aligned} \tag{22}$$

where the rate constant

$$R_0 = N\log_2\rho + \log_2\det\left(\left(\underline{\mathbf{V}}_{\mathrm{R}}^{(M)}\right)^H\underline{\mathbf{V}}_{\mathrm{R}}^{(M)}\right) + 2\log_2\det\left(\underline{\mathbf{\Sigma}}^{(M)}\right)$$

only depends on the SNR ρ and the fixed geometry of the UE array. Therefore, maximizing the achievable rate (8) in the near-field region is equivalent to maximizing the determinant related to the diagonal matrix $\mathbf{D}_{\mathrm{T}}$ and the Vandermonde matrix $\underline{\mathbf{V}}_{\mathrm{T}}^{(M)}$, which are respectively given by

$$\det\left(\mathbf{D}_{\mathrm{T}}\mathbf{D}_{\mathrm{T}}^H\right) = \prod_{m=1}^{M}\frac{1}{r_m^2}, \tag{23}$$

and

$$\det\left(\left(\underline{\mathbf{V}}_{\mathrm{T}}^{(M)}\right)^H\underline{\mathbf{V}}_{\mathrm{T}}^{(M)}\right) = \prod_{1\le i<j\le M}\left(\sin\phi_j-\sin\phi_i\right)^2, \tag{24}$$

with range[2] $\phi_i = \varphi_i - \theta_{\mathrm{UE}} \in [-\pi/2, \pi/2]$.

[2]The range is chosen based on practical considerations, since UE arrays are typically oriented so that their main boresight approximately faces the serving BS array.

Denote the antenna position in the *angular domain* as

$$\begin{aligned} s_m &= \sin\left(\varphi_m - \theta_{\mathrm{UE}}\right) \\ &= \sin\left(\arctan\left(\frac{x_{\mathrm{BS}}^{(m)} - x_0}{y_0}\right) - \theta_{\mathrm{UE}}\right). \end{aligned} \tag{25}$$

Then, the distance term r_m in (23) can then be expressed by

$$r_m^2 = \frac{y_0^2}{\cos^2\varphi_m} = \frac{y_0^2}{1-\tilde{s}_m^2}, \tag{26}$$

where $\tilde{s}_m = \sin\varphi_m = \sin\left(\arcsin s_m + \theta_{\mathrm{UE}}\right)$. By substituting (26) into (23), problem $\mathcal{P}_1$ is equivalent to

$$\begin{aligned} \mathcal{P}_2: \max_{\mathbf{s}} \quad & 2\sum_{1\le i<j\le M} \log_2\left(s_j - s_i\right) + \sum_{m=1}^{M} \log_2\left(1-\tilde{s}_m^2\right) \\ \text{s.t.} \quad & s_{\min} = s_1 < s_2 < \cdots < s_M = s_{\max}, \end{aligned} \tag{27}$$

where $s_{\min}$ and $s_{\max}$ are given by setting $x_{\mathrm{BS}}^{(m)}$ in (25) as $-A/2$ and $A/2$, respectively. Problem $\mathcal{P}_2$ is known as the *weighted Fekete problem* [15, p. 114, Ch. III] with weighting function

$$w(s) = 1 - \tilde{s}^2 = 1 - \sin^2\left(\arcsin s + \theta_{\mathrm{UE}}\right), \tag{28}$$

which generalizes the classical Fekete problem by incorporating a position-dependent weighting function.

Remark 1. *In classical potential theory, the Fekete problem seeks the optimal placement of M electric charges on a compact set to maximize logarithmic potential energy [15]. In the presence of an external electric field, this framework extends to the weighted Fekete problem, where optimal distribution of charges achieves a balance between mutual repulsion and external influence. In the context of near-field communication with MAs, the mutual coupling among antennas corresponds to the internal interaction, while the field induced by the UE array serves as the external field. Accordingly, the positions of M MAs have to be delicately optimized to obtain a state of equilibrium between these two forces.*

IV. Proposed Optimal Antenna Positions

In this section, we first analyze the convexity of problem $\mathcal{P}_2$, which guarantees the uniqueness of the optimal solution and enables its numerical computation using existing mathematical tools. To reduce the computational complexity introduced by the intrinsic iterative procedures involved in the optimization algorithm, we further propose a greedy framework to calculate the asymptotically optimal antenna positions efficiently.

A. Optimal Solution

We first reveal the convexity of problem $\mathcal{P}_2$ by the following lemma.

Lemma 1. *Problem $\mathcal{P}_2$ is a concave problem with a unique solution of position vector* $\mathbf{s}$.

Proof: Let $\mathbf{J}$ be the Hessian matrix of the objective function $J(\mathbf{s})$ in (27), whose elements are given by

$$\mathbf{J}[m,n] = \frac{\partial^2 J}{\partial s_m \partial s_n}, \tag{29}$$

the quadratic form of $\mathbf{J}$ with arbitrary non-zero vector $\mathbf{v} = [v_1, v_2, \cdots, v_M]^T$ is then given by

$$\begin{aligned} Q(\mathbf{v}) &= \mathbf{v}^T\mathbf{J}\mathbf{v} \\ &= -\sum_{1\le i<j\le M} \frac{\left(v_i - v_j\right)^2}{\left(s_i - s_j\right)^2} - \sum_{m=1}^{M} \frac{(2+\tan\phi_m \sin 2\varphi_m) v_m^2}{(1-s_m^2)\cos^2\varphi_m}, \end{aligned} \tag{30}$$

where the factor $1/\ln 2$ is dropped for brevity. The quadratic form $Q(\mathbf{v})$ is strictly negative with $\phi_m \in [-\pi/2, \pi/2]$ for any given $\mathbf{v} \neq \mathbf{0}$. Therefore, the Hessian matrix $\mathbf{J}$ is negative definite, i.e., $\mathbf{J} \prec 0$, which establishes that $J(\mathbf{s})$ is strictly concave. Moreover, as the feasible set defined by $s_1 < s_2 < \cdots < s_M$, where s_1 and s_M are fixed, is a convex set, $\mathcal{P}_2$ is a convex optimization problem. This guarantees the existence and uniqueness of the global maximum, which can be obtained numerically by existing toolboxes such as CVX [16]. ■

B. Greedy Algorithm

However, solving $\mathcal{P}_2$ with standard convex optimization is computationally demanding, as gradient evaluations involve nested iterations that scale poorly with the number of antennas. Additionally, incorporating additional physical constraints, such as minimum antenna spacing [8]–[10], further compromises the convexity of the problem, thereby exacerbating the computational intractability. To cope with these challenges, we develop a greedy framework that decomposes $\mathcal{P}_2$ into a sequence of simpler sub-problems, each solved iteratively to obtain locally optimal positions. This procedure corresponds to the well-known *Leja sequence* [17], which has been shown to asymptotically converge to the optimal solution of the weighted Fekete problem [15].

Suppose that $m-1 < M$ positions $\{s_i^\star\}_{i=1}^{m-1}$ have been determined, when we determine the m-th position s_m, the objective function will be augmented by the pair-wise distance contribution and the weighting function-related contribution, according to problem $\mathcal{P}_2$, respectively. For the pair-wise distance part, the additional contribution of the new antenna element at position s is given by

$$J_{\mathrm{D}}(s) = 2\sum_{i=1}^{m-1} \log_2\left|s_i^\star - s\right|. \tag{31}$$

For the weighting function part, the additional contribution is given by

$$J_{\mathrm{W}}(s) = \log_2\left(1 - \sin^2\left(\arcsin s + \theta_{\mathrm{UE}}\right)\right). \tag{32}$$

Therefore, the m-th point can be obtained by

$$s_m^\star = \arg\max_{s\in\mathcal{S}} \left(J_{\mathrm{D}}(s) + J_{\mathrm{W}}(s)\right), \tag{33}$$

where

$$\mathcal{S} = \{s \in \mathbb{R} \mid s_1 < s < s_M\} \tag{34}$$

is the feasible region. Note that it is not strictly necessary to exclude the previously selected $m-1$ points from the feasible region, since the distance-related objective $J_{\mathrm{D}}(s)$ approaches negative infinity at those locations. However, in practical scenarios, the minimum spacing between adjacent

Algorithm 1 Greedy Antenna Position Design

Input: The number of antenna elements M, the antenna spacing thresholds ϵ, the aperture of BS array A, the centroid position (x_0, y_0), and the azimuth angles θ_{UE} of the UE array.

Output: The positions $\{x_{\text{BS}}^{(m)}\}_{m=1}^{M}$ of M antenna elements solving $\mathcal{P}_2$.

1: Determine $s_1^\star = s_1$ and $s_2^\star = s_M$ according to (27).
2: **for** $m = 3, \cdots, M$ **do**
3: Update the feasible region $\mathcal{S}_m$ according to (35).
4: Determine the position of the m-th antenna element $s_m^\star$ according to (33) over $\mathcal{S}_m$.
5: **end for**
6: Sort the positions $\{s_i^\star\}_{i=1}^{M}$ in ascending order as $\{s_i\}_{i=1}^{M}$.
7: Obtain the coordinate on the x-axis by (37).
8: **return** The positions $\{x_{\text{BS}}^{(m)}\}_{m=1}^{M}$ on the x-axis.

antenna elements should not be lower than a given threshold ϵ to avoid the severe mutual coupling effect. Incorporating such a constraint, the feasible region at the m-th step is given by

$$\mathcal{S}_m = \{s \in \mathbb{R} \mid s_1 < s < s_M\} \setminus \bigcup_{i=1}^{m-1} B_\epsilon, \tag{35}$$

where

$$B_\epsilon = \left\{ \sin(\arctan(\tfrac{x-x_0}{y_0}) - \theta_{\text{UE}}) \middle| |x - x_{\text{BS}}^{(m)}| < \epsilon \right\} \tag{36}$$

represents the set of s values corresponding to the ϵ-neighborhood around $x_{\text{BS}}^{(m)}$ on the x-axis. After obtaining the positions of antenna elements $\{s_m\}_{m=2}^{M-1}$ in the angular domain, according to (25), the coordinates of antennas can be further obtained by

$$x_{\text{BS}}^{(m)} = x_0 + y_0 \tan(\theta_{\text{UE}} + \arcsin s_m). \tag{37}$$

The detailed procedure is summarized in **Algorithm 1**.

V. Numerical Results

A. System Setup

Throughout the simulation, we deploy $M = 128$ MAs on the BS array and $N = 8$ antennas on the UE array. The carrier frequency is set as $f_c = 10$ GHz, and the aperture of the BS array is around $A \approx 2$ m. The centroid of the UE array is selected randomly from the near-field region with centroid distance $r_0 = \sqrt{x_0^2 + y_0^2}$ and centroid angle $\varphi_0 \in [-\pi/3, \pi/3]$, respectively, and the azimuth angle of the UE θ_{UE} is selected ensuring condition $\varphi_M - \pi/2 < \theta_{\text{UE}} < \varphi_1 + \pi/2$. The UE array adopts a ULA configuration with standard spacing $d = \lambda/2$. As the received power is significantly affected by the distance in the near-field region, we normalize the SNR to $\rho = 20$ dB.

In the simulation, we mainly consider the following schemes for comparison.

- **ULA**. Both BS and UE are employing ULAs with standard spacing d.

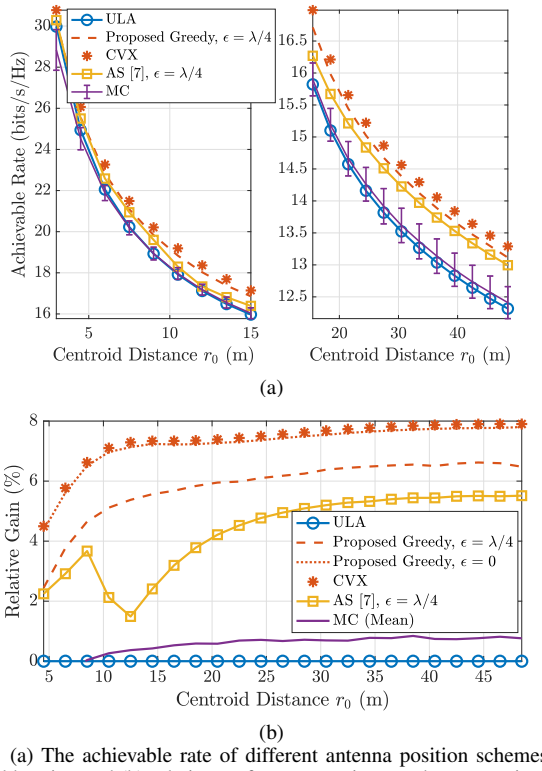

Fig. 2. (a) The achievable rate of different antenna position schemes in the near-field region and (b) relative performance gain over the conventional ULA scheme within $r_0 \in [5, 50]$ m.

- **Monte-Carlo (MC)**. During each simulation step, 2000 random antenna position patterns for the BS array are generated randomly without spacing constraint.
- **Antenna Selection (AS)** [7]. Antenna positions are selected from $G = 2M$ uniform grids with the minimum spacing $\epsilon = \lambda/4$.
- **Proposed Greedy**. The BS array obtains the antenna positions by adopting the proposed greedy scheme with $\epsilon = \lambda/4$.
- **Proposed Convex Optimization Approach**. The antenna positions are obtained by solving the concave problem $\mathcal{P}_2$ with mathematical tools such as CVX without a spacing constraint.

B. Simulation Results

We first investigate the achievable rate of different antenna position schemes with varying distances $r_0 \in [5, 50]$ m in the near-field region. As shown in Fig. 2(a), the proposed schemes consistently attain the highest achievable rate, where the greedy algorithm (in dashed line) closely matches the performance of the CVX-based scheme (in $*$ marker). In contrast, although the AS scheme exhibits comparable performance to the proposed method at shorter distances, its performance gap gradually widens as r_0 increases. As the centroid distance grows, the near-field effect becomes less significant, resulting in a general decline in achievable rates across all schemes. However, as shown in Fig. 2(b), the relative gain of the proposed schemes over the conventional ULA scheme gradually increases, sustaining a stable gain of

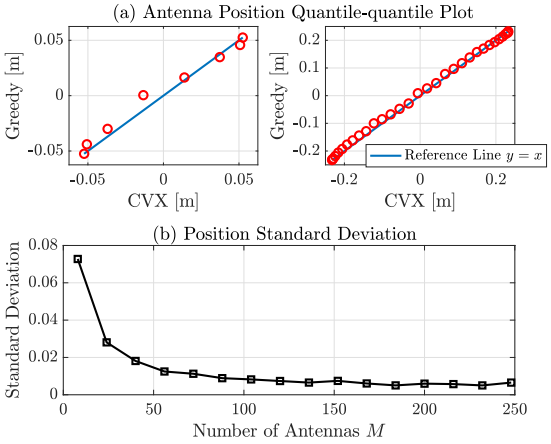

Fig. 3. (a) Quantile-quantile plot and (b) the standard deviations of antenna positions.

TABLE I
COMPUTATIONAL COMPLEXITY AND AVERAGE RUNTIME

Methods	**Computational Complexity** ($\mathcal{O}$)	**Ave. Runtime (ms)**	
		$M = 16$	$M = 128$
AS [7]	$MG^2(N^3+M^2N^2)$	47.4	3.38×10^3
Prop. CVX*	$\sim M^{4.5}$	6.42×10^3	3.47×10^5
Prop. Greedy	GM^2	2.19	94.1

* Using interior-point method.

around 8%, which verifies its superiority in practical near-field communications.

In Fig. 2(b), it is also shown that the proposed greedy algorithm ($\epsilon = 0$) achieves almost identical performance as the CVX approach. Hence, we further investigate the asymptotic relationship between the solutions of these two methods. As shown in Fig. 3(a), the horizontal axis corresponds to the antenna positions obtained by CVX, while the vertical axis corresponds to the results from the greedy algorithm. The line $y = x$ serves as the reference line, and the deviation of scatter points from this line directly indicates the discrepancy between the two solutions. For the case $M = 8$ on the left-hand-side, a noticeable offset can be observed for some antenna elements, implying non-negligible difference between the obtained solutions; For the case $M = 32$ on the right-hand-side, such deviations become much insignificant. Fig. 3(b) further illustrates the standard deviation between the two solutions, showing that the greedy algorithm rapidly approaches the optimal target as M grows, and achieves relative convergence quickly around $M = 64$.

We finally evaluate the computational complexity of the proposed methods, as summarized in Table I, where G denotes the number of searching grids in the comparison algorithms. Although the AS method provides acceptable performance, its extremely high computational burden makes it unsuitable for large-scale scenarios. The CVX-based optimization attains the optimal solution, but still suffers from prohibitively high complexity. In contrast, the proposed greedy algorithm offers significantly reduced complexity by 35 times. This implies the advantage of the proposed greedy algorithm as an effective yet scalable design method for near-field LoS communication with massive MAs.

VI. CONCLUSIONS

In this paper, we developed a novel greedy framework to solve the achievable rate maximization problem in the near-field LoS scenario. By transforming the antenna positions into the angular domain, we formulated the problem into a weighted Fekete problem, whose unique optimal solution can be asymptotically approximated by the proposed greedy strategy. Numerical results demonstrated the superiority in asymptotic optimality and the computational efficiency of the proposed algorithm.

REFERENCES

[1] Z. Wang *et al.*, "A tutorial on extremely large-scale MIMO for 6G: Fundamentals, signal processing, and applications," *IEEE Commun. Surveys Tuts.*, vol. 26, no. 3, pp. 1560–1605, thirdquarter 2024.

[2] E. Björnson *et al.*, "Towards 6G MIMO: Massive spatial multiplexing, dense arrays, and interplay between electromagnetics and processing," *arXiv preprint*, Jan. 2024.

[3] X. Yu, J.-C. Shen, J. Zhang, and K. B. Letaief, "Alternating minimization algorithms for hybrid precoding in millimeter wave MIMO systems," *IEEE J. Sel. Topics Signal Process.*, vol. 10, no. 3, pp. 485–500, Apr. 2016.

[4] L. Zhu, W. Ma, and R. Zhang, "Movable-antenna array enhanced beamforming: Achieving full array gain with null steering," *IEEE Commun. Lett.*, vol. 27, no. 12, pp. 3340–3344, Dec. 2023.

[5] K.-K. Wong, A. Shojaeifard, K.-F. Tong, and Y. Zhang, "Fluid antenna systems," *IEEE Trans. Wireless Commun.*, vol. 20, no. 3, pp. 1950–1962, Mar. 2021.

[6] Z. Ding, R. Schober, and H. Vincent Poor, "Flexible-antenna systems: A pinching-antenna perspective," *IEEE Trans. Commun.*, pp. 1–1, Mar. 2025, *early access*.

[7] S. Yang, W. Lyu, B. Ning, Z. Zhang, and C. Yuen, "Flexible precoding for multi-user movable antenna communications," *IEEE Wireless Commun. Lett.*, vol. 13, no. 5, pp. 1404–1408, May 2024.

[8] Y. Wu, D. Xu, D. W. K. Ng, W. Gerstacker, and R. Schober, "Globally optimal movable antenna-enabled multiuser communication: Discrete antenna positioning, power consumption, and imperfect CSI," *IEEE Trans. Commun.*, pp. 1–1, 2025, *early access*.

[9] Y. Zhang *et al.*, "Movable antenna-aided hybrid beamforming for multi-user communications," *IEEE Trans. Veh. Technol.*, pp. 1–6, 2025, *early access*.

[10] J. Ding, Z. Zhou, X. Shao, B. Jiao, and R. Zhang, "Movable antenna-aided near-field integrated sensing and communication," *IEEE Trans. Wireless Commun.*, pp. 1–1, 2025, *early access*.

[11] K. Chen, C. Qi, Y. Hong, and C. Yuen, "REMAA: Reconfigurable pixel antenna-based electronic movable-antenna arrays for multiuser communications," *IEEE Trans. Commun.*, vol. 73, no. 11, pp. 12 913–12 928, Nov. 2025.

[12] S. Liu, X. Yu, Z. Gao, J. Xu, D. W. K. Ng, and S. Cui, "Sensing-enhanced channel estimation for near-field XL-MIMO systems," *IEEE J. Sel. Areas Commun.*, vol. 43, no. 3, pp. 628–643, Mar. 2025.

[13] J. C. Ruiz-Sicilia, M. D. Renzo, P. Mursia, A. Kaushik, and V. Sciancalepore, "Spatial multiplexing in near-field line-of-sight MIMO communications: Paraxial and non-paraxial deployments," *IEEE Trans. Green Commun. Netw.*, vol. 9, no. 1, pp. 338–353, Mar. 2025.

[14] P. Wang, Y. Li, Y. Peng, S. C. Liew, and B. Vucetic, "Non-uniform linear antenna array design and optimization for millimeter-wave communications," *IEEE Trans. Wireless Commun.*, vol. 15, no. 11, pp. 7343–7356, 2016.

[15] E. B. Saff and V. Totik, *Logarithmic Potentials with External Fields*. Springer Cham, 2024.

[16] I. CVX Research, "CVX: Matlab software for disciplined convex programming, version 2.1," https://cvxr.com/cvx, Aug. 2014.

[17] F. Leja, "Sur certaines suites liées aux ensembles plans et leur application à la représentation conforme," *Ann. Polon. Math.*, vol. 4, no. 1, pp. 8–13, 1957.